Suppression of PIK3CA-driven epileptiform activity by acute pathway control

Achira Roy[1,*], Victor Z. Han[1,2], Angela M. Bard[1], Devin T. Wehle[1,3], Stephen E. P. Smith[1,4], Jan-Marino Ramirez[1,4,5,6], Franck Kalume[1,5,7,†], Kathleen J. Millen[1,4,†,*]

[1]Center for Integrative Brain Research, Seattle Children's Research Institute, Seattle, Washington, USA; [3]Graduate Program in Neuroscience and Departments of [2]Biology,[4]Pediatrics, [5]Neurological Surgery, [6]Physiology and Biophysics, and [7]Pharmacology, University of Washington, Seattle, Washington, USA;

[†]contributed equally

*Correspondence: Kathleen J. Millen, PhD
Seattle Children's Research Institute,
Center for Integrative Brain Research
1900 9th Avenue, Mailstop: JMB-10, Seattle, WA, USA. ZIP: 98101
Email: kathleen.millen@seattlechildrens.org; Tel: +1-206-884-3225

Achira Roy, PhD
Seattle Children's Research Institute
Center for Integrative Brain Research
1900 9th Avenue, Mailstop: JMB-10, Seattle, WA, USA. ZIP: 98101
Email: achira.roy@gmail.com; Tel: +1-206-884-5490

Number of Figures: 4

Number of Extended Data Figures: 8

Number of Extended Data Table: 1

Words: 2316

ABSTRACT

A significant proportion of epilepsy patients is non-responsive to conventional anti-seizure medications. Many of these patients harbor causative mutations in the PI3K-AKT-MTOR signaling pathway[1-5]. Understanding mutation-specific pathophysiology is critical for developing molecularly targeted therapies. Here we identify physiological mechanisms underlying dysregulation of neuronal excitability and its acute attenuation in a mouse model expressing patient-related activating mutation in *Pik3ca*, that encodes the p110α catalytic subunit of PI3K[6]. We show that Pik3ca-dependent hyperexcitability in hippocampal pyramidal neurons is mediated by changes in non-synaptic, cell-intrinsic properties, involving calcium and potassium channels. Our results also suggest a potential reason behind Pik3ca-dependent epileptic intractability. Further, we report that acute inhibition of PI3K or AKT, but not MTOR, suppresses the intrinsic epileptiform nature of the mutant neurons. This study therefore represents an important advance towards repurposing anti-cancer therapeutics to treat intractable epilepsy.

KEYWORDS:

PI3K, epilepsy, mouse model, BKM120, RAD001, AZD5363, preclinical, pyramidal neuron, hippocampus, electrophysiology

Mutations in the PI3K-AKT-MTOR signaling pathway, long studied for roles in cancer[7,8], also cause clinically important developmental brain overgrowth syndromes. Affected individuals display phenotypes ranging from dysplastic megalencephaly, hemimegalencephaly and focal cortical dysplasia, as well as comorbidities including hydrocephalus, autism and intellectual disability[3,5,9]. These mutations also cause focal epilepsy, representing 25-50% of all cases of intractable (treatment-resistant) epilepsy in children[1-4,10]. Traditionally, anti-seizure drugs targeting generic ion channels are identified by evoking acute seizures in wild-type rodents[11-13], which do not mimic clinical epilepsies associated with specific genetic mutations and hence are largely ineffective. Since PI3K pathway mutations are now known to cause intractable epilepsy, repurposing pathway-targeted anti-cancer drugs offers a tantalizing opportunity to fundamentally shift the therapeutic approach towards intractable epilepsy. Presently, the MTOR inhibitor rapamycin and its analogs are the sole pathway-related drugs used clinically to treat epilepsy, primarily in patients with rare *TSC1/2* deletion mutations which enhance downstream MTOR signaling[9,10,14]. Yet, these treatments remain effective only to a modest degree, suggesting that MTOR activation may not be the sole arm of this complex signaling pathway accounting for all PI3K pathway-driven epilepsies[6,15,16]. Here we assess acute mechanisms driving epileptiform activity in *Nestin-cre;Pik3ca*^{E545K} mouse model harboring patient-related activating mutation in *Pik3ca*, encoding the p110α catalytic subunit of PI3K[6]. We report that Pik3ca overactivation causes intrinsic neuronal changes leading to hyperexcitability. We further establish that this epileptiform activity is acutely dependent on AKT, but not MTOR, regulation. Our study defines key aspects of acute neuronal dysregulation in an

important genetic epilepsy model, that can be leveraged to potentially repurpose the available PI3K pathway inhibitors against intractable epilepsy.

Mutant CA1 shows hyperactivity *in vivo*

Pik3ca mutant mouse models recapitulate patient phenotypes including brain overgrowth, cortical dysplasia, hydrocephalus and epilepsy, with phenotypic severity dependent on the mutant allele and its time of activation[6,17]. Moreover, this developmental epilepsy is dissociable from dysmorphology and acutely suppressible by 1-hour *in vivo* administration of the pan-PI3K inhibitor BKM120[6,18]. To identify the underlying dynamic mechanisms, we performed *in vivo* and *in vitro* electrophysiological studies primarily focused on hippocampal pyramidal neurons, since the connection between epilepsy and hippocampal pathophysiology is well documented in patients and model systems, including ours[6,19-22].

We investigated *in vivo* changes in the hippocampal CA1 network activity of ~P70 *Nestin-cre;Pik3ca*^{E545K} mutant mice relative to control littermates using local field potential (LFP) recordings, while simultaneously monitoring cortical surface activity by electrocorticography (ECoG). These recordings showed spontaneous interictal spike activity either restricted to the cortex or the hippocampus exclusively, or concurrent to the two regions in the mutant mice (Fig. 1a-c, Extended Data Fig. 1a-d). A broad spectrum of spike patterns was observed, consisting of single or groups of interictal spikes, the simplest identifiable unit of epileptiform activity[23], as well as trains of sharp spikes, low-frequency slow waves or high-frequency low-amplitude “brushing events”. These epileptiform events were observed exclusively in the mutant mice. Within the

mutant group, the event frequency was significantly higher in the hippocampus than in the neocortex (Fig. 1d). Power spectrum analyses revealed that the mutant hippocampi exhibit significantly higher power in the gamma frequency bands (Fig. 1e-h), which is often indicative of seizure onset[24,25]. These observations indicate that Pik3ca overactivation caused significant neural hyperexcitability in our mice, predominantly in the hippocampus.

Mutant CA1 has elevated network excitability

To assess the physiological aspects of Pik3ca-driven epilepsy at the tissue level, we performed hippocampal extracellular field recordings in acute forebrain slices. First, we conducted these recordings in P16-20 CA1 pyramidal layer, across a potassium concentration gradient in the recording buffer ([K^+]: 3 mM to 12 mM; Fig. 2a-c). This standard model shifts wild-type neuronal network from a silent state to tonic spiking and then to bursting, followed by a depolarization block at very high levels of [K^+], thus mimicking a seizure-like response[26]. Compared to controls, mutant slices exhibited a narrow range of hypersynchronous bursting and an elevated mean baseline measured from the integrated trace, especially from 8mM to 12mM [K^+] (Fig. 2b,c; Extended Data Fig. 2a). Mutant slices also showed significantly enhanced relative peak amplitudes (at 8-9 mM [K^+]; Extended Data Fig. 2b). Thus, the mutation lowers the excitability threshold and a depolarization block is reached faster than in controls. Further, acute extracellular application of BKM120 suppressed the hypersynchronous ictal bursts in the mutant CA1 field in 20-30 min, with minimal physiological effect on control brains (Fig. 2d,e). These data provide evidence of a Pik3ca-driven active mechanism.

Mutant CA1/3 neurons are hyperexcitable

Next, we investigated mechanisms driving the mutant epileptiform activity at the cellular level, using whole-cell patch-clamp recordings from CA1 and CA3 pyramidal neurons in P16-20 control and mutant brains (Fig. 3a). Silent and spontaneously firing, tonic and burst-generating neurons were detected in both control and mutant slices (Fig. 3b,c). However, mutant slices had a significantly higher proportion of burst-generating cells in both regions and lower proportion of tonic-firing cells in mutant CA1 compared to controls (Fig. 3d,e). Additionally, we observed significantly higher tonic spike frequencies in mutant CA1 and CA3 and higher burst frequency in mutant CA1, compared to controls (Fig. 3f,g). Burst-generating cells demonstrated multiple burst types. Specifically, we identified burst clusters and two types of plateau-bursts; paroxysmal depolarization shift (PDS) and non-PDS waveforms (Extended Data Fig. 3a). We defined burst cluster as a multi-spike burst activity of random nature without a plateau potential; these were only observed in mutant slices (Extended Data Fig. 3b). Plateau-bursts with depolarization shift resulting in sodium-spike inactivation were termed as PDS “bursting cells”. These depolarization shifts have previously been implicated as the intracellular correlate of *in vivo* interictal spikes[23,27-29]. We defined non-PDS bursts as those where plateau potential developed in absence of prominent sodium-spike inactivation. No significant differences between control and mutant hippocampal pyramidal cells were observed with respect to average burst duration or inter-burst interval (Extended Data Fig. 3c-e). However, the plateau potential shift (PPS), defined here as the difference of the steady state plateau potential and the

resting membrane potential (RMP), was significantly larger in mutant CA1 but not in CA3, relative to respective controls (Fig. 3h,h'). This was despite similar RMP across control and mutant hippocampal neurons (Extended Data Fig. 4a-c). The evoked current-clamp recordings further validated the spontaneous activity results, especially by displaying significantly higher percentage of burst-generating pyramidal neurons in the mutant hippocampus (Fig. 3i-m). Incidentally, no significant difference in membrane intrinsic properties like input resistance, rheobase current and burst-threshold current, as well as evoked tonic spike frequencies (for the tested 0-90pA range), was observed between control and mutant cells (Extended Data Table 1; Extended Data Fig. 4d-f). But the decay time constant for mutant CA3 neurons was significantly longer than that in mutant CA1 and control groups (Extended Data Table 1). With similar resistance, this implied that mutant CA3 neurons have higher membrane capacitance than other cell groups. Together, these data demonstrate that Pik3ca overactivation results in intracellular hyperexcitability, with some distinct cell type-specific effects.

To determine whether the Pik3ca-related hyperexcitability is driven by altered synaptic interactions or other intrinsic properties, we assessed the effects of channel and receptor blockers on mutant hippocampal physiology. Blocking glutamatergic inputs by extracellular administration of NMDA and non-NMDA receptor-antagonists, 3-((±)2-carboxypiperazin-4yl) propyl-1-phosphate (CPP) and 6-cyano-7-nitroquinoxaline-2,3-dione (CNQX) respectively, had no overt physiological effect on the majority of mutant hippocampal neurons (Extended Data Fig. 5a-c,e,f,h-k). Similarly, blocking inhibitory synaptic inputs with gabazine did not significantly alter the mutant firing patterns, spike frequencies or PPS (Extended Data Fig. 5d,g,l). The proportion of mutant CA1 neurons

affected by these channel blockers was comparatively less than that in CA3. Our data lead to the important conclusion that Pik3ca-driven epileptiform activity is primarily not dependent on synaptic transmission. In contrast, inhibition of calcium (Ca^{2+})-dependent inward current by extracellular cadmium (Cd^{2+}) attenuated the paroxysmal bursts and reduced burst frequency and PPS (Extended Data Fig. 6a-d), indicating a calcium channel-dependent mechanism underlying the Pik3ca-dependent epileptiform activity. Intracellular cesium blocked potassium channels and related currents, altering the intrinsic firing pattern in both control and mutant hippocampal slices. Specifically, compared to regular baseline recordings, intracellular cesium considerably reduced the proportion of tonic-firing cells in both CA1 and CA3 (Extended Data Fig. 6e-h, compare to Fig. 3d,e). Unlike the spontaneous recordings, intracellular cesium prompted the burst frequency in mutant CA1 to normalize and in mutant CA3 to significantly rise, relative to respective controls (Extended Data Fig. 6i, compare to Fig. 3g). Intracellular cesium also normalized the mutant PPS to control levels (Extended Data Fig. 6j, compare to Fig. 3h). No overt effect on RMP or input resistance was seen in cesium-treated control and mutant cells (Extended Data Fig. 6k,l). We conclude that Pik3ca-related epileptiform activity is primarily caused by a complex set of altered non-synaptic cell-intrinsic properties.

Acute treatment with PI3K pathway drugs

The acute suppression of epileptiform activity in *Nestin-cre;Pik3ca*^{E545K} mice by BKM120, both *in vivo*[6] and at the tissue level, prompted us to dissect the downstream pathway dynamics using inhibitors at the cellular level, in order to coarsely determine

their mechanistic roles and identify new therapeutic targets to treat intractable epilepsy (Fig. 4a). Acute extracellular administration of BKM120 or the pan-AKT inhibitor AZD5363[30] resulted in a large-scale and significant alteration of firing pattern, frequencies and a relative reduction of PPS, sometimes leading to gradual silencing of the recorded neurons (Fig. 4b-i'). Neither drug had any significant effect on neuronal RMP or tonic rheobase current (Extended Data Fig. 7a,b,e,f). In contrast to BKM120, acute AKT downregulation by AZD5363 significantly reduced the mutant burst duration and inter-burst interval (Extended Data Fig. 7c,d,g,h). Further, AZD5363 altered the physiology of all mutant CA3 neurons much faster (~8 min) than BKM120 (~32 min); however, both drugs changed the intracellular activity of ~50% cells within 4 min (Extended Data Fig. 7i,j). AZD5363 also blocked spontaneous bursts in mutant neurons faster than BKM120 (Extended Data Fig. 7k). Thus, acute regulation of both PI3K and AKT activity directly suppressed *Pik3ca*^{E545K}-driven epileptiform neuronal activity. In contrast, acute administration of the MTOR inhibitor RAD001 (everolimus)[15,31] showed no overt effect on the mutant RMP, tonic or burst firing patterns, frequencies, average PPS, burst duration, inter-burst interval and rheobase current (Fig. 4j-m, Extended Data Fig. 8a-d). This was despite western blot confirmation that acute treatment of forebrain slices with RAD001 modulated direct downstream targets of MTOR (Extended Data Fig. 8e-g). In summary, our study demonstrates that epileptiform activity caused by Pik3ca overactivation is based on multiple intrinsic electrophysiological characteristics that are acutely modifiable by downregulating PI3K and AKT activity, but not MTOR.

DISCUSSION

Activating mutations in the PI3K-AKT-MTOR pathway commonly cause pediatric intractable epilepsy[5,10]; yet the underlying mechanisms remain largely undefined. Using our *Nestin-cre;Pik3ca*^{E545K} model, we now establish that Pik3ca-dependent neuronal hyperexcitability in hippocampal pyramidal neurons is driven primarily by intrinsic neuronal mechanisms. Acute attenuation of epileptiform activity by inhibiting AKT but not MTOR also reveals a previously unknown role of PI3K signaling in neuronal homeostasis. Our mouse model of human intractable epilepsy is now validated across whole animal, tissue and cellular levels.

Epileptiform activity is typically marked by increased tonic depolarizations and/or quasiperiodic bursts, mediated by intrinsic membrane properties, ephaptic or synaptic/circuit-level interactions[23,32]. We confirmed enhanced interictal spike frequency and diverse, synchronized epileptiform spike patterns in the mutant brains *in vivo*, predominantly in the hippocampus. This is consistent with studies of *PIK3CA* variants in brain tumors and mouse models with patient-related *Pik3r2* mutations, which are less common causes of intractable epilepsy[33,34]. Our *in vitro* analyses revealed intracellular correlates of epileptiform activity and enhanced firing frequencies in mutant hippocampal pyramidal neurons. Relative to controls, mutant neurons exhibited significantly higher proportions of bursting cells and higher heterogeneity in burst patterns, including burst clusters and PDSs. A prior study showed that human neurons from surgically resected neocortical samples of pediatric patients with focal cortical dysplasia (FCD) exhibited remarkably similar burst characteristics[27]. These samples were not genotyped; however, since most cases of FCD and epilepsy result from

variants in PI3K pathway genes[3], such cross-species phenotypic correlation is remarkable and emphasizes the clinical relevance of our mouse model.

The PI3K-AKT-MTOR pathway is also known to influence synaptogenesis and neuronal plasticity[35]. For example, neocortical samples from patient and mouse models with *TSC* mutations exhibit synaptic input-mediated epileptogenic hyperexcitability[36]. However, blocking glutamatergic (NMDA and non-NMDA) or GABAergic synaptic inputs showed no significant effect on the neuronal activity in our mutant brain slices. We do acknowledge that altered neuronal circuitry may be relevant to Pik3ca-mediated epilepsy. But our data demonstrate that altered synaptic interactions are not primary mediators of dynamic hippocampal neuronal hyperexcitability. Significant reduction of burst-generating cells, burst frequency and PPS by blocking voltage-dependent calcium or potassium channels indicate that *Pik3ca*^{E545K}-driven epileptiform activity is predominantly mediated by multiple altered cell-intrinsic properties. Yet, some cell-intrinsic properties, such as burst frequencies, PPS and time constants, are distinctly different between mutant CA1 and CA3 neurons. Since all neurons do not react uniformly to either pathway overactivation or Cd^{2+}/Cs^{+}-dependent channel inhibition, current anti-seizure drugs that typically target single ion channels are unlikely to work in entirety, potentially explaining epileptic intractability in this patient population.

PI3K-AKT-MTOR inhibitors developed to treat cancer potentially represent novel anti-seizure therapeutics[18,37-39]. Rapamycin and its analogs, that are currently in clinical use to treat epilepsy in TSC patients, curbed epileptiform activity in mouse models harboring *TSC1/2*, *MTOR* or *PTEN* mutations when administered long-term (>7-day)[9,10,14,40,41]. In contrast, we show acute inhibition of epileptiform activity by BKM120

in vitro, confirming our previous *in vivo* finding[6]. We also demonstrate that acute AKT inhibition with AZD5363 has similar effects. This first preclinical study using AZD5363 to treat epilepsy shows that acute Pik3ca-driven epileptiform mechanism is predominantly AKT-dependent, limiting roles for other PI3K targets. Intriguingly, rapamycin analog RAD001 had minimal acute effect in our model. While elevated MTOR activity is known to be epileptogenic[9,10], our data suggest that alternate PI3K-AKT targets acutely regulate neuronal hyperexcitability. This study establishes an important foundation to determine active pathway-driven cellular mechanisms and to assess the plethora of available PI3K pathway inhibitors, facilitating new molecularly rational therapeutic interventions for intractable epilepsy.

REFERENCES

1. Bast, T., Ramantani, G., Seitz, A. & Rating, D. Focal cortical dysplasia: prevalence, clinical presentation and epilepsy in children and adults. *Acta Neurol Scand* **113**, 72-81 (2006).
2. Blumcke, I.*, et al.* The clinicopathologic spectrum of focal cortical dysplasias: a consensus classification proposed by an ad hoc Task Force of the ILAE Diagnostic Methods Commission. *Epilepsia* **52**, 158-174 (2011).
3. Mirzaa, G., Roy, A., Dobyns, W.B., Millen, K.J., Hevner, R.F. Hemimegalencephaly and Dysplastic Megalencephaly' in *Developmental Neuropathology* (ed. Adle-Biassette H, G.J., Harding BN) (Wiley Blackwell, 2018).
4. Stafstrom, C.E. & Carmant, L. Seizures and epilepsy: an overview for neuroscientists. *Cold Spring Harb Perspect Med* **5**(2015).
5. Dobyns, W.B. & Mirzaa, G.M. Megalencephaly syndromes associated with mutations of core components of the PI3K-AKT-MTOR pathway: PIK3CA, PIK3R2, AKT3, and MTOR. *Am J Med Genet C Semin Med Genet* **181**, 582-590 (2019).
6. Roy, A.*, et al.* Mouse models of human -related brain overgrowth have acutely treatable epilepsy. *Elife* **4**(2015).
7. Madsen, R.R. PI3K in stemness regulation: from development to cancer. *Biochemical Society transactions* **48**, 301-315 (2020).
8. Yang, J.*, et al.* Targeting PI3K in cancer: mechanisms and advances in clinical trials. *Mol Cancer* **18**, 26 (2019).
9. Crino, P.B. The mTOR signalling cascade: paving new roads to cure neurological disease. *Nat Rev Neurol* **12**, 379-392 (2016).
10. Kim, J.K. & Lee, J.H. Mechanistic Target of Rapamycin Pathway in Epileptic Disorders. *J Korean Neurosurg Soc* **62**, 272-287 (2019).
11. Wilcox, K.S., West, P.J. & Metcalf, C.S. The current approach of the Epilepsy Therapy Screening Program contract site for identifying improved therapies for the treatment of pharmacoresistant seizures in epilepsy. *Neuropharmacology* **166**, 107811 (2020).
12. Kehne, J.H., Klein, B.D., Raeissi, S. & Sharma, S. The National Institute of Neurological Disorders and Stroke (NINDS) Epilepsy Therapy Screening Program (ETSP). *Neurochemical research* (2017).
13. Barker-Haliski, M. & White, H.S. Validated animal models for antiseizure drug (ASD) discovery: Advantages and potential pitfalls in ASD screening. *Neuropharmacology*, 107750 (2019).
14. *Developmental Epilepsy - From Clinical Medicine to Neurobiological Mechanisms*, (World Scientific, 2019).
15. Cho, C.H. Frontier of epilepsy research - mTOR signaling pathway. *Experimental & molecular medicine* **43**, 231-274 (2011).
16. Meng, X.F., Yu, J.T., Song, J.H., Chi, S. & Tan, L. Role of the mTOR signaling pathway in epilepsy. *J Neurol Sci* **332**, 4-15 (2013).
17. Roy, A.*, et al.* PI3K-Yap activity drives cortical gyrification and hydrocephalus in mice. *Elife* **8**(2019).
18. Maira, S.M.*, et al.* Identification and characterization of NVP-BKM120, an orally available pan-class I PI3-kinase inhibitor. *Mol Cancer Ther* **11**, 317-328 (2012).
19. Roy, A., Millen, K.J. & Kapur, R.P. Hippocampal granule cell dispersion: a non-specific finding in pediatric patients with no history of seizures. *Acta Neuropathol Commun* **8**, 54 (2020).
20. Chatzikonstantinou, A. Epilepsy and the hippocampus. *Front Neurol Neurosci* **34**, 121-142 (2014).

21. Mazumder, A.G., Patial, V. & Singh, D. Mycophenolate mofetil contributes to downregulation of the hippocampal interleukin type 2 and 1beta mediated PI3K/AKT/mTOR pathway hyperactivation and attenuates neurobehavioral comorbidities in a rat model of temporal lobe epilepsy. *Brain Behav Immun* **75**, 84-93 (2019).
22. Berdichevsky, Y.*, et al.* PI3K-Akt signaling activates mTOR-mediated epileptogenesis in organotypic hippocampal culture model of post-traumatic epilepsy. *J Neurosci* **33**, 9056-9067 (2013).
23. McCormick, D.A. & Contreras, D. On the cellular and network bases of epileptic seizures. *Annual review of physiology* **63**, 815-846 (2001).
24. Hughes, J.R. Gamma, fast, and ultrafast waves of the brain: their relationships with epilepsy and behavior. *Epilepsy Behav* **13**, 25-31 (2008).
25. Lee, S.A., Spencer, D.D. & Spencer, S.S. Intracranial EEG seizure-onset patterns in neocortical epilepsy. *Epilepsia* **41**, 297-307 (2000).
26. Filatov, G., Krishnan, G.P., Rulkov, N.F. & Bazhenov, M. Dynamics of epileptiform activity in mouse hippocampal slices. *J Biol Phys* **37**, 347-360 (2011).
27. Marcuccilli, C.J.*, et al.* Neuronal bursting properties in focal and parafocal regions in pediatric neocortical epilepsy stratified by histology. *Journal of clinical neurophysiology : official publication of the American Electroencephalographic Society* **27**, 387-397 (2010).
28. Kubista, H., Boehm, S. & Hotka, M. The Paroxysmal Depolarization Shift: Reconsidering Its Role in Epilepsy, Epileptogenesis and Beyond. *Int J Mol Sci* **20**(2019).
29. Tryba, A.K.*, et al.* Role of paroxysmal depolarization in focal seizure activity. *J Neurophysiol* **122**, 1861-1873 (2019).
30. Davies, B.R.*, et al.* Preclinical pharmacology of AZD5363, an inhibitor of AKT: pharmacodynamics, antitumor activity, and correlation of monotherapy activity with genetic background. *Mol Cancer Ther* **11**, 873-887 (2012).
31. Krueger, D.A.*, et al.* Everolimus for subependymal giant-cell astrocytomas in tuberous sclerosis. *N Engl J Med* **363**, 1801-1811 (2010).
32. Dudek, F.E., Yasumura, T. & Rash, J.E. 'Non-synaptic' mechanisms in seizures and epileptogenesis. *Cell biology international* **22**, 793-805 (1998).
33. Yu, K.*, et al.* PIK3CA variants selectively initiate brain hyperactivity during gliomagenesis. *Nature* **578**, 166-171 (2020).
34. Shi, X.*, et al.* PIK3R2/Pik3r2 Activating Mutations Result in Brain Overgrowth and EEG Changes. *Ann Neurol* **88**, 1077-1094 (2020).
35. Sanchez-Alegria, K., Flores-Leon, M., Avila-Munoz, E., Rodriguez-Corona, N. & Arias, C. PI3K Signaling in Neurons: A Central Node for the Control of Multiple Functions. *Int J Mol Sci* **19**(2018).
36. Wang, Y.*, et al.* Neocortical hyperexcitability in a human case of tuberous sclerosis complex and mice lacking neuronal expression of TSC1. *Ann Neurol* **61**, 139-152 (2007).
37. Cardamone, M.*, et al.* Mammalian target of rapamycin inhibitors for intractable epilepsy and subependymal giant cell astrocytomas in tuberous sclerosis complex. *J Pediatr* **164**, 1195-1200 (2014).
38. Lindhurst, M.J.*, et al.* Repression of AKT signaling by ARQ 092 in cells and tissues from patients with Proteus syndrome. *Sci Rep* **5**, 17162 (2015).
39. Zou, Z., Tao, T., Li, H. & Zhu, X. mTOR signaling pathway and mTOR inhibitors in cancer: progress and challenges. *Cell Biosci* **10**, 31 (2020).
40. Curatolo, P. & Moavero, R. mTOR inhibitors as a new therapeutic option for epilepsy. *Expert Rev Neurother* **13**, 627-638 (2013).
41. Lasarge, C.L. & Danzer, S.C. Mechanisms regulating neuronal excitability and seizure development following mTOR pathway hyperactivation. *Frontiers in molecular neuroscience* **7**, 18 (2014).

FIGURES

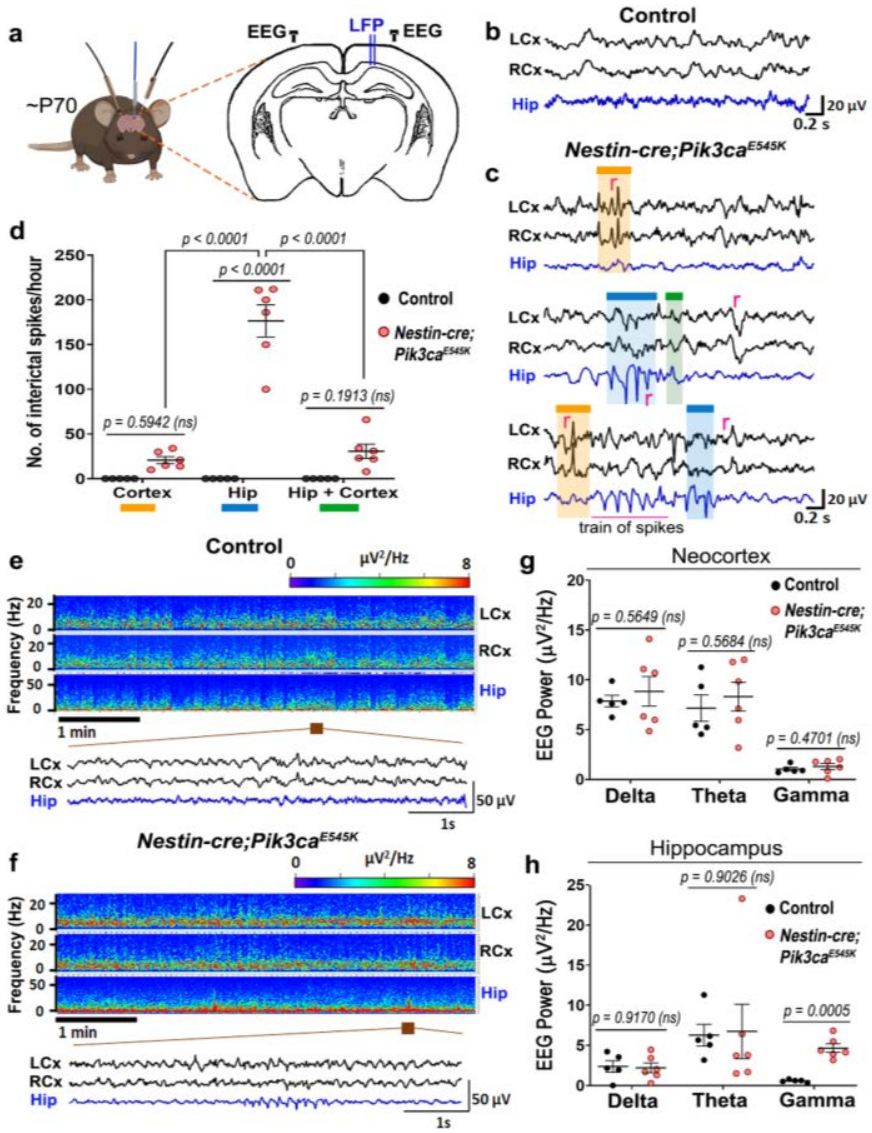

Fig. 1: *Nestin-cre;Pik3ca^{E545K}* mutant brains show higher neural excitability

(**a**) Schematic shows electrode placement for EEG-ECoG recordings in ~P70 *Nestin-cre;Pik3ca^{E545K}* and control littermates. LFP, local field potential. (**b,c**) Compared to controls, the mutants showed significantly higher frequency of regional (r) spikes and train of spikes/polyspikes in neocortex (black traces) and hippocampus (blue traces). (**d**) In the mutant, interictal spike frequency was significantly higher in hippocampus (blue box), compared to those generated in neocortex (orange box) or generalized in both

regions (green box) ($F=46.65$, degrees of freedom (df)=27). (**e,f**) Power spectrum analysis displayed increased activity in mutant, as emphasized in the representative magnified segments. (**g,h**) Mutant hippocampus demonstrated significant higher activity in the gamma frequency range ($F=3.932$, df=27; neocortex: $F=26.93$, df=27). Data is represented as mean ± SEM scatter plots; differences were considered significant at $p<0.05$; ns, not significant. Scalebars: 0.2s,20μV (b,c); 1s,50μV (e,f).

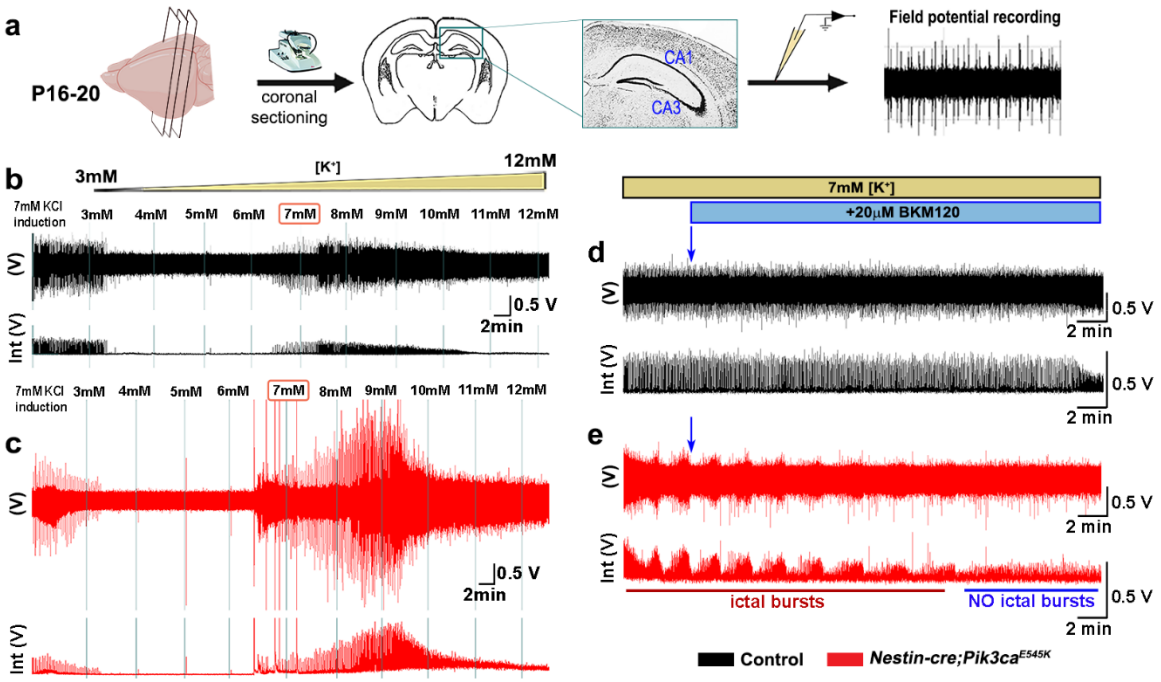

Fig. 2: Extracellular mutant CA1 recordings demonstrate hyper-synchronization (**a**) Schematized flowchart summarizes the acute coronal brain slicing for extracellular field potential recording. (**b,c**) Representative control (black) and mutant (red) voltage and integrated voltage traces across a [K^+] gradient; comparison indicated significantly higher excitability in the mutant brain. (**d,e**) Acute extracellular BKM120 administration at constant 7mM [K^+] aCSF suppressed synchronized ictal bursts in mutant CA1 field within ~20-30min, with minimal effect on the control hippocampal slices. Scalebars: 2min,0.5V (b-e).

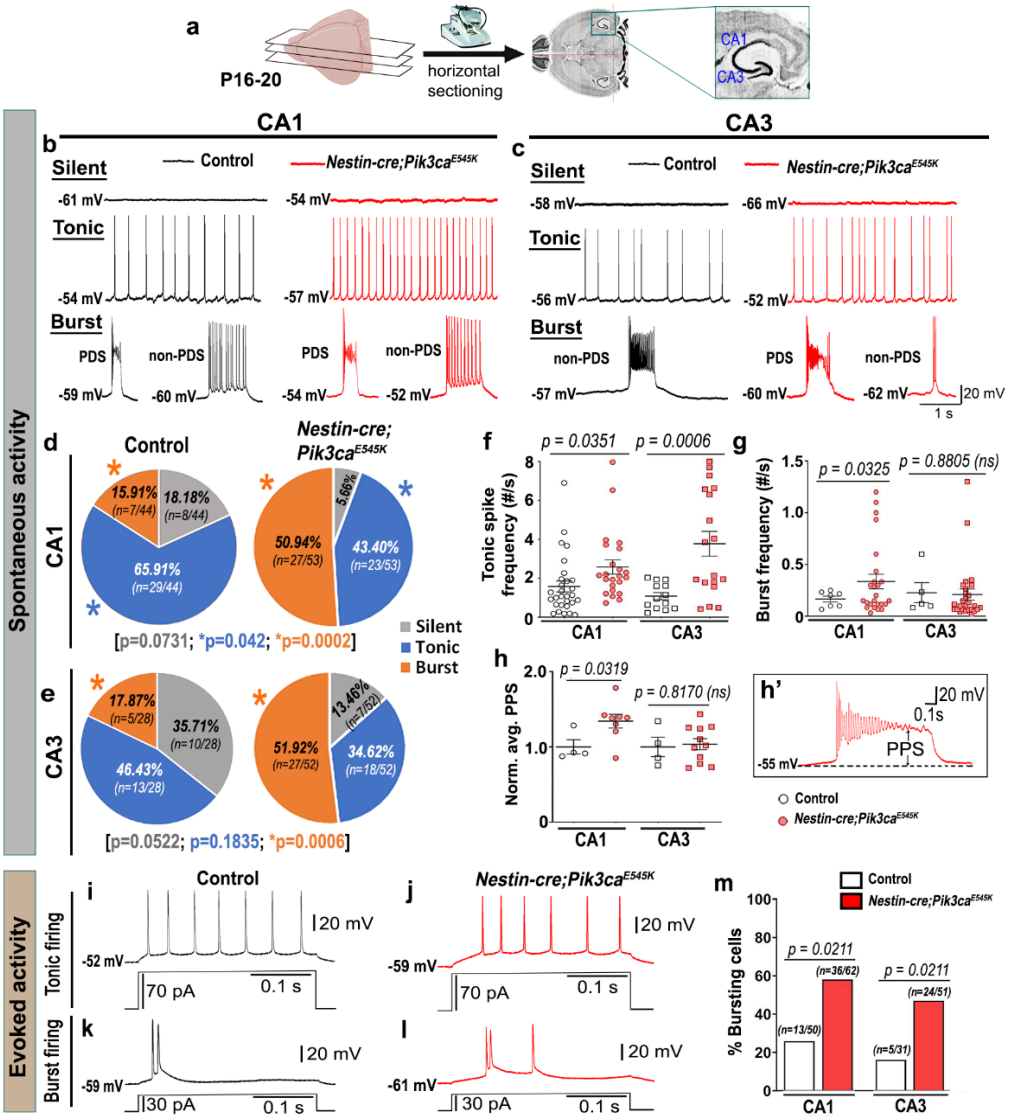

386 **Fig. 3: Mutant hippocampal neurons produce increased epileptiform burst activity**

387 (**a**) Flowchart shows acute horizontal brain slicing for whole-cell recording. (**b-e**) Traces
388 represent silent, tonic and burst categories of CA1 and CA3 neurons based on
389 spontaneous cellular activity; respective pie charts marked proportion of recorded cells.
390 Mutant CA1 and CA3 exhibited significantly higher proportions of burst-firing cells
391 compared to controls. Significantly fewer tonic-firing cells were observed in mutant CA1.
392 (**f,g**) relative to controls, spontaneous tonic spike frequencies were significantly higher
393 in mutant CA1 (t=2.175, df=43.71) and CA3 (t=4.063, df=19.78) cells; burst frequency

was significantly higher in mutant CA1 (CA1: t=2.244, df=29.38; CA3: t=0.1561, df=6.754). (**h**) Plateau potential shift (PPS) in mutant bursting cells, as depicted in (**h'**), was significantly higher in CA1 (t=2.586, df=8.118) but similar in CA3 (t=0.2436, df=5.110), compared to respective controls. (**i-l**) Representative evoked voltage traces of control and mutant showed tonic and burst firing in response to current steps. (**m**) Evoked recording also marked significantly higher bursting cell proportions in the mutant. Data is represented as pie charts, % bar graphs and mean ± SEM scatter plots; differences were considered significant at $p<0.05$; ns, not significant. Scalebars: 1s,20mV (b,d); 0.1s,20mV (h', i-l).

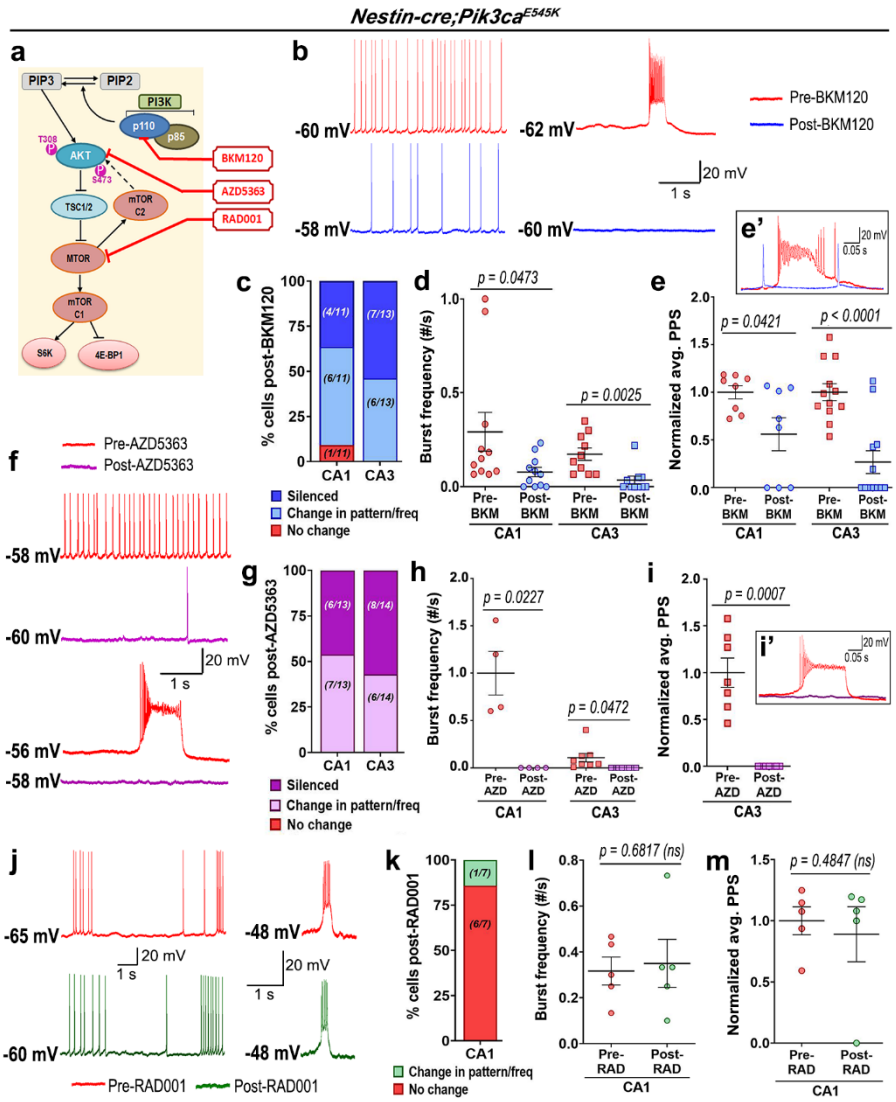

Fig. 4: Acute inhibition of Pik3ca or Akt suppresses hyperactivity in mutant cells

(**a**) Schematic of simplified PI3K-AKT-MTOR pathway, marking targets of action for BKM120, AZD5363 and RAD001. Representative traces demonstrate differential action of BKM120 (**b**), AZD5363 (**f**) and RAD001 (**j**) on *Nestin-cre;Pik3ca*^{E545K} hippocampal neurons, ranging from being unaffected to change in frequency/pattern to silencing, as quantitated respectively in (**c,g,k**). (**d,e,h,i**) BKM120 and AZD5363 significantly reduced mutant burst frequency (BKM120: F=8.937, df=38; AZD5363: F=43.50, df=20) and PPS (BKM120: F=24.39, df=36; AZD5363: t=6.386, df=6) in both CA1 and CA3. (**e',i'**) Insets

show activity traces of mutant bursting cell before (red) and after BKM120 (blue) or AZD5363 (pink) administration. (**l,m**) Acute RAD001 treatment had no overt effect on the mutant burst frequency (t=0.4414, df=4) or PPS (t=0.7692, df=4). Data is represented as % bar graphs and mean ± SEM scatter plots; differences were considered significant at $p<0.05$; ns, not significant. Scalebars: 1s,20mV (b,f,j); 0.05s,20mV (e',i').

METHODS

Mice

The following mouse lines were used: *Nestin-cre* (Jackson Labs, Bar Harbor, Maine, USA; Stock #003771, RRID: IMSR_JAX:003771), conditional *Pik3ca*^{E545K} knock-in[42]. *Nestin-cre* and *Pik3ca*^{E545K} mouse lines were maintained in C57BL/6 and FVB backgrounds respectively. We have designated *Nestin-cre;Pik3ca*^{E545K} conditional mutant mice as "*Pik3ca* mutants" or "mutants" throughout the manuscript.

All mice were housed in Optimice cages with aspen bedding at the Seattle Children's Research Institute's specific pathogen-free (SPF) vivarium facility (light "ON": 6am – 8pm). Noon of the day of vaginal plug was designated as embryonic day 0.5 (E0.5). The day of birth was designated as postnatal day 0 (P0). Genotyping by PCR was done using separate sets of primers for the *Cre* coding region and the *Pik3ca*^{E545K} allele, as previously described[6]. All mouse procedures were approved and conducted in accordance with the guidelines laid down by the Institutional Animal Care and Use Committees (IACUC) of Seattle Children's Research Institute, Seattle, WA, USA.

In vivo electrophysiology

5 control and 6 *Nestin-cre;Pik3ca*^{E545K} mutant mice (age: ~P70) were used for *in vivo* regular and depth-electrode electrophysiology experiments. We saw no sex-dependent data correlation[6].

Electrode implantation surgery: Mice underwent survival surgery to implant ECoG, EMG, and hippocampal depth electrodes under isoflurane anesthesia using similar

procedures as reported in our prior work[6,43]. The ECoG electrodes consisted of silver wire (diameter: 130 µm bare; 180 µm coated) attached to micro screws. The ECoG electrodes were implanted bilaterally through small cranial burr holes above the somatosensory cortices. A similar reference electrode was placed above the cerebellum following the same procedure. The depth electrodes were made of 2 fine twisted tungsten wires (30um nylon coated, California fine wire) and implanted in the hippocampal CA1 region (coordinates: -2.0 mm anteroposterior, 1.5 mm mediolateral, 1.9 mm dorsoventral in reference to bregma) to record local field potential (LFP). All electrodes were connected to interface connector and fixed to the skull with dental cement (Lang Dental Manufacturing Co., Inc., Wheeling, IL). Mice were allowed to recover from surgery for 2-3 days.

Video, electroencephalagraphy and local field potential (Video-EEG-LFP) recording: Simultaneous video-EEG-LFP recordings were collected from conscious mice on PowerLab 8/35 and 16/30 data acquisition units, using LabChart 7.3.3 software (AD Instruments, Colorado Spring, USA). ~6 hours of baseline ECoG tracings were visually reviewed for the presence of spontaneous epileptiform events, as previously studied[44-46]. All bioelectrical signals were acquired at a 20 KHz sampling rate. The ECoG signals were processed with a 1-70 Hz bandpass filter and the LFP signal with a 5 Hz high-pass filter. Interictal spikes were identified as transient, clearly distinguished from background activity, with pointed peak and slow wave. Myoclonic seizures were identified as shock-like muscular jerks on video, associated with a spike or polyspike-wave complex on EEG. Power spectral analysis and visual inspection of the data were conducted to

characterize the EEG activity in different frequency bands and identify epileptiform event on the ECoG and local CA1 field recordings using the Labchart 8.2 software.

***In vitro* electrophysiology**

Slice preparation: Postnatal (P16-20) pups were anesthetized briefly in a closed chamber by administering isoflurane (5% flow rate) or CO_2 (constant flow rate: 10-30% of chamber vol/min); then perfused transcardially with ice-cold low Na^+-buffer ("slicing solution," which included the following: 252 mM sucrose, 2 mM KCl, 2 mM $MgCl_2$, 2.6 mM $CaCl_2$, 1.2 mM NaH_2PO_4, 26 mM $NaHCO_3$, and 15 mM glucose, with the pH adjusted to 7.4 and the osmolarity to 310 ± 5 mOsm). Brain was dissected out by separating the head and cutting along the skull sutures using fine scissors and forceps. The forebrain was isolated in ice-cold, oxygenated (95% O_2, 5% CO_2) slicing solution. A slanted (~15° from vertical) agar block was secured on a specimen tray as a support for the brain during slicing. The isolated forebrain was glued with cyanoacrylate in the orientation depending on the type of slices we wanted; and then placed in the vibratome for slicing. Slicing was proceeded until hippocampal landmark was visible. For coronal slices (extracellular recordings), the forebrain was placed such that its antero-posterior (A-P) axis was perpendicular to the specimen tray/vibratome blade, and olfactory bulb distal to the tray surface. For horizontal slices (whole-cell recordings), the forebrain was oriented such that it's A-P axis was parallel to the specimen tray and ventral side (hippocampal side) was on the top, distal to the tray surface. Once the hippocampus became visible, thick, acute slices (thickness: 350μm for extracellular recordings, 200-250μm for whole-cell patch clamp recordings) were taken and incubated in ice-cold

slicing solution continuously oxygenated with 95% O_2/5% CO_2. After cutting, slices were immediately returned to the same solution and maintained in a warm bath (28 ± 0.5°C) for recovery. After 30 min, they were transferred into regular artificial cerebrospinal fluid (aCSF), composed of the same components as slicing solution except for the replacement of sucrose with 126 mM NaCl. Slices were then kept at room temperature, continuously superfused with oxygenated aCSF, until recording. Given that *Pik3ca*^{E545K} mutant is megalencephalic, a greater number of hippocampal/forebrain sections were obtained. However, care was taken so that the dorso-ventral plane(s) used for recording was always comparable between control and mutant slices. No randomization was used. Tissue collection was not performed blind since the mice were subjected to genotyping and drug administration.

Recording: Slices were transferred into a recording chamber, continuously superfused with oxygenated aCSF, for extracellular or intracellular whole-cell recordings. The pClamp software suite (Molecular Devices; RRID:SCR_011323) was used for data acquisition and analysis. Signals were amplified (MultiClamp 700A, Axon Instruments, Molecular Devices, USA), digitized (D1322A, Axon Instruments, Molecular Devices, USA), and stored in a computer for post-hoc analysis.

a) Extracellular recording: To determine if hippocampal neuronal populations in *Pik3ca*^{E545K} mutants have different electrochemical signatures than controls, extracellular population recordings were performed on CA1 hippocampal pyramidal neuronal layer in acute 350 µm-thick coronal brain slices of ~P16-20 *Pik3ca*^{E545K} mutant and control littermates (n=6). To induce epileptiform activity in the slices, we increased potassium concentration ($[K^+]$)[47,48] from 3 mM to 12 mM, in 1mM increments at 30°C.

This standard model induces wild-type neurons to transition from a silent neuronal state to tonic spiking and then to bursting, followed by depolarization block at very high $[K^+]$[26].

b) Intracellular recording: Horizontal hemi-forebrain slices with prominent hippocampus were used for intracellular whole-cell visual patch-clamp experiments. Slices transferred to the recording chamber were maintained at 30-34°C, constantly superfused with oxygenated aCSF. Borosilicate glass capillaries/pipettes for patch-clamp recording had electrode resistance (R_e) optimally kept around 5-8 MΩ, after being filled with internal solution containing the following: potassium gluconate (~132 mM), KCl (5 mM), HEPES (10 mM), EGTA (5 mM), $CaCl_2.H_2O$ (0.5 mM), $MgCl_2$ (2 mM), disodium phosphocreatine (5 mM), disodium-ATP (4 mM), trisodium-GTP (0.5 mM), EGTA (5 mM). Cells were visualized under brightfield optics using the 40X water-immersion objective of an upright microscope (Olympus, BX51WI). The patch electrode was advanced toward the target cells by a micromanipulator (MP-225, Sutter Instrument Company, USA) and 1 GΩ seal was established, typically by a small negative pressure, with the membrane ruptured by gentle suction and/or zap pulses. Whole-cell patch-clamp recording was performed from cell bodies of pyramidal neurons of hippocampal CA1 and CA3 respectively. Following intracellular recording protocols were also used:

i. Spontaneous gap-free recordings in current (I)-clamp: cells were typically tested at resting conditions (without current injection) unless noticed otherwise.
ii. Evoked I-clamp steps protocol: current steps start at -50 pA, incremental 10 pA, duration; 300 ms; 15 steps (-90 to +50 pA) were recorded across experiments.

Acute chemical assays

Channel blockers: Chemicals inhibiting specific ion channels were introduced in the bath/recording chamber during *in vitro* whole-cell recordings to compare different components contributing to the neural activity in control and *Pik3ca*^{E545K} mutant mice. To block all fast-synaptic excitatory transmission, 3-((±)2-carboxypiperazin-4yl) propyl-1-phosphate (CPP, NMDA receptor antagonist, 20 μM; Tocris Bioscience, UK) and 6-cyano-7-nitroquinoxaline-2,3-dione (CNQX, AMPA/kainite (non-NMDA) receptor antagonist, 20 μM, diluted in DMSO; Alomone Labs, Israel) were introduced in the bath[49,50]. SR95531 hydrobromide (Gabazine, $GABA_A$ receptor antagonist, 10 μM, Tocris Bioscience, UK) were used to block inhibitory synaptic transmission. Divalent cation Cd^{2+} ($CdCl_2$, 100 μM; Sigma-Aldrich, USA)[51] was used to depress synaptic transmission and block inward calcium-selective current, isolating the outward K^+ current. To block voltage-dependent K^+ channels, intracellular administration of cesium[52] was done by replacing potassium gluconate with cesium gluconate in the internal solution while maintaining the same osmolarity.

PI3K pathway drugs: Drugs regulating PI3K pathway were added to the circulating recording buffer, thus getting acutely administered in the brain slice placed in the recording chamber. For protein analyses, these were added at identical concentration to the brain slices incubated in oxygenated aCSF for ~1hr. The following PI3K pathway inhibitors were dissolved in 100% DMSO and used *in vitro*: pan-PI3K inhibitor BKM120 (Buparlisib; Novartis, Switzerland; working concentration: ~3.5 μM); pan-AKT inhibitor AZD5363 (Capivasertib; Selleckchem, USA; working concentration: 0.5 μM); MTOR

inhibitor RAD001 (Everolimus, Chem Express Cat# 159351-69-6; working concentration: 0.52 µM).

Western blotting

Horizontal forebrain slices from 5 control and 5 mutant mice were obtained and recovered in oxygenated aCSF as detailed above. Slices showing nice hippocampal morphology were selected, treated for 1 hour with DMSO, BKM120, AZD5363 and RAD001 respectively, in the same concentrations used for recording. The treated slices were then flash-frozen in liquid nitrogen and stored at -80°C for post-processing. These brain slices were lysed in NP-40 lysis buffer (150 mM NaCl, 50 mM Tris (pH 7.4), 1% NP-40, 10 mM NaF, 2 mM sodium orthovanadate + protease/phosphatase inhibitor cocktails [Sigma, USA]). Samples were normalized to equal protein concentrations (0.333 mg/ml) using Pierce BCA protein assay (Thermo Fisher Scientific, USA). Standards were made through serial dilutions of 10 mg/ml BSA. Samples were diluted into a final concentration of 1x Laemmli sample buffer and boiled at 95°C for ten minutes. 7.5% 10-well gels were prepared, and samples were run at 120V for 1.5 hours. Gels were transferred onto polyvinylidene difluoride (Millipore) membranes and run either overnight at 25V or for 2 hours at 60V. Membranes were blocked in 4% milk in TBST (0.05 M Tris, 0.15 M NaCl, pH7.2, 0.1% (v/v) Tween20) for one hour at room temperature, and primary antibodies were applied overnight at 4°C in blocking medium. Primary antibodies for western blots were diluted as follows: rabbit anti-Phospho-AKT Ser473 (D9E) (Cell Signaling Technology, USA; RRID: AB_2797780; 1:2000), mouse anti-Pan-AKT (40D4) (Cell Signaling Technology, USA; Cat# 2920; 1:2000), rabbit anti-

Phospho-S6 Ribosomal Protein Ser235/236 (Cell Signaling Technology, USA; RRID: AB_2721245, 1:2000), mouse anti-S6 Ribosomal Protein (54D2) (Cell Signaling Technology, USA; RRID: AB_2238583, 1:1000), rabbit anti-beta(β)-Actin (GeneTex, USA; RRID: AB_1949572, 1:10000). After washing and probing respectively with goat anti-rabbit (RRID: AB_2313567) and anti-mouse (RRID: AB_10015289) horseradish peroxidase (HRP)-conjugated secondary antibodies (1:10000; Jackson ImmunoResearch Labs, USA), blots were imaged using Femto chemiluminescent detection reagents (Thermo Fisher Scientific, USA; Cat# 34095) in a FluorChem R western blot imaging system (ProteinSimple, Bio-Techne, USA). 8-bit images were used as a representative western blot. 16-bit images were used to quantify the intensity of each band using ImageJ v1.53. Regions of interest were drawn in each sample's lane. After quantifying the lane in a histogram, the peak representing the band of interest was isolated and the area of the region was measured as the band's quantification.

Quantitative Analysis

Number of mice used was consistent with previous experiments completed and published by us and other investigators. For extracellular field potential analyses, baseline potential from integrated traces were measured for each [K^+] and normalized to the value at 3 mM for each slice per genotype; relative peak amplitude was similarly measured for control and mutant slices for 3,7,8,9 mM of [K^+]. In whole-cell patch-clamp recording, plateau potential shift (PPS) was calculated by subtracting the baseline potential from the highest plateau/burst potential in a paroxysmal depolarizing event. Burst duration and inter-burst interval were measured as shown in Extended Data Fig. 3

and averaged across multiple bursts per cell. Input resistance was measured from evoked current-clamp recordings by dividing the voltage difference (measured at -10pA to -30pA I-steps) by the current interval (20pA). The decay membrane time constant was obtained by recording the membrane response to 20pA hyperpolarizing current pulses (300 ms duration, 1 Hz) and fitting the response to a single exponential curve. We chose 20pA of hyperpolarizing current because such a current intensity did not produce sag. Evoked spike frequencies and rheobase current were calculated exclusively from tonic-firing cells. Burst threshold current was calculated from burst-generating cells as the first current step which induced burst. *In vitro* electrophysiological analyses were performed using Clampfit 10.7 and 11 (pClamp, Molecular Devices, USA). For Western Blots, each band intensity was recalculated relative to its respective β-actin band intensity, and then normalized across average intensity per protein lane. Normalized ratios of phosphoproteins over total proteins were thereafter obtained.

Statistical significance was assessed using 2-tailed unpaired t-tests with Welch's correction (EEG power analyses, whole-cell RMP, burst duration, inter-burst interval, Cd^{2+} data), 2-tailed paired t-tests (field potential baseline measurement, rheobase current, drug-treated analyses) and ANOVA followed by Tukey post-tests (EEG interictal spike frequency, field potential relative peak amplitude; whole-cell tonic spike and burst frequencies, cell proportions, PPS, evoked spike frequency and time constant; Western blots). Normal distribution was assumed for the data analyses, when required. For EEG-ECoG-LFP experiments, quantitative and statistical data analysis was performed in Labchart 8.2 software (AD Instruments, Colorado Spring, USA) and

Igor Pro 6.37 (WaveMetrics Inc., USA); final graphs were made in GraphPad Prism v7.0 (GraphPad Software Inc., San Diego, USA). For the remaining data, statistical analyses and graph plotting were done using GraphPad Prism v7.0 and Microsoft Excel. Differences were considered significant at $p<0.05$.

ARRIVE guidelines have been followed for reporting work involving animal research.

42. Robinson, G.*, et al.* Novel mutations target distinct subgroups of medulloblastoma. *Nature* **488**, 43-48 (2012).
43. Bolea, I.*, et al.* Defined neuronal populations drive fatal phenotype in a mouse model of Leigh syndrome. *Elife* **8**(2019).
44. Kalume, F. Sudden unexpected death in Dravet syndrome: respiratory and other physiological dysfunctions. *Respir Physiol Neurobiol* **189**, 324-328 (2013).
45. Liautard, C.*, et al.* Hippocampal hyperexcitability and specific epileptiform activity in a mouse model of Dravet syndrome. *Epilepsia* **54**, 1251-1261 (2013).
46. Roy, A.*, et al.* Mouse models of human PIK3CA-related brain overgrowth have acutely treatable epilepsy. *eLife* **4:e12703** (2015).
47. Borck, C. & Jefferys, J.G. Seizure-like events in disinhibited ventral slices of adult rat hippocampus. *J Neurophysiol* **82**, 2130-2142 (1999).
48. Leschinger, A., Stabel, J., Igelmund, P. & Heinemann, U. Pharmacological and electrographic properties of epileptiform activity induced by elevated K+ and lowered Ca2+ and Mg2+ concentration in rat hippocampal slices. *Exp Brain Res* **96**, 230-240 (1993).
49. Lehmann, J.*, et al.* CPP, a selective N-methyl-D-aspartate (NMDA)-type receptor antagonist: characterization in vitro and in vivo. *J Pharmacol Exp Ther* **240**, 737-746 (1987).
50. Lester, R.A., Quarum, M.L., Parker, J.D., Weber, E. & Jahr, C.E. Interaction of 6-cyano-7-nitroquinoxaline-2,3-dione with the N-methyl-D-aspartate receptor-associated glycine binding site. *Mol Pharmacol* **35**, 565-570 (1989).
51. Boissard, R.*, et al.* The rat ponto-medullary network responsible for paradoxical sleep onset and maintenance: a combined microinjection and functional neuroanatomical study. *Eur J Neurosci* **16**, 1959-1973 (2002).
52. Covey, E., Kauer, J.A. & Casseday, J.H. Whole-cell patch-clamp recording reveals subthreshold sound-evoked postsynaptic currents in the inferior colliculus of awake bats. *J Neurosci* **16**, 3009-3018 (1996).

Acknowledgements/Funding

We thank Suzanne J. Baker for gifts of mouse lines (*Nestin-cre* and *Pik3ca*^{E545K}); Leon Murphy (Novartis) for BKM120; Rory M. Murphy, Amanda P. Tran Hartman, Nikhil Sahai and Jiyun Ryu for technical assistance; Aguan D. Wei and Paul Wakenight for discussions. This work is funded by the NIH grants 1R01NS099027 (K.J.M.), R01MH113545 (S.E.P.S.), R01NS102796 (F.K.), and CURE Sleep and Epilepsy Grant (F.K.).

Authors' contributions

A.R., F.K., J.M.R. and K.J.M. contributed to the study conception and design. A.R., V.H., A.M.B., D.T.W. and F.K. contributed to the data collection. A.R. and F.K. contributed to *in vitro* and *in vivo* data analyses respectively. D.T.W. and S.E.P.S. contributed to Western blot data analyses and interpretation. A.R., F.K., J.M.R., K.J.M. contributed to the overall data interpretation. S.E.P.S., F.K. and K.J.M. provided the funding resources. A.R. wrote the first draft of the manuscript and others commented on previous versions of the manuscript. All authors read and approved the final manuscript.

Competing Interests Statement. All authors read and approved the final manuscript. None of the authors have competing interests.

Ethics

Animal experimentation: All animal experimentation was conducted in accordance with the guidelines laid down by the Institutional Animal Care and Use Committees (IACUC)

of Seattle Children's Research Institute, Seattle, WA, USA (protocol IDs: IACUC00006 (K.J.M.); IACUC00058 and IACUC00084 (J.M.R.); IACUC00108 (F.K.)).

ADDITIONAL INFORMATION

Supplementary Information is available for this paper

Correspondence and requests for materials should be addressed to A.R. or K.J.M.

Availability of data and material: All data generated or analyzed during this study are included in this article (and its extended data files).